ChemComm

COMMUNICATION

View Article Online
View Journal

Cite this: DOI: 10.1039/d6cc00357e

Received 19th January 2026,
Accepted 18th February 2026

DOI: 10.1039/d6cc00357e

rsc.li/chemcomm

"Inverted" hysteresis in a bilayer Fe(II) spin crossover system

Aleksandra Tołoczko, Marcin Kaźmierczak, Vladyslav Maliuzhenko, Miłosz Siczek, Marek Weselski and Robert Bronisz *

The coupling between the spin state and the complex motion of the individual alkyl chains results in a unique thermal hysteresis exhibiting an "inverted" loop. Specifically, the high-spin (HS) → low-spin (LS) transition upon cooling occurs at a higher temperature than the LS → HS transition upon heating.

Thermally induced spin crossover (SCO) is an entropy-driven phenomenon, meaning that lowering the temperature decreases the relative contribution of the entropic term, leading to stabilization of the LS form.[1,2] Nevertheless, in addition to conventional, entropy-driven SCO,[3,4] significant structural changes may dominate the electronic ΔS_{el} and vibrational ΔS_{vib} contributions related to metal–ligand distance variations, and give rise to the so-called reverse SCO.[5–7] Such behavior has been observed for systems incorporating ligands with built-in conformationally labile fragments, particularly alkyl chains. It is worth emphasizing that the introduction of a conformationally labile fragment may result in unconventional transitions, combining features of both normal and reverse SCO.[8–12]

In both normal and reverse SCO, the external stimulus induces SCO at a critical temperature T_c. Reversal of the stimulus direction causes the reverse transition to occur only after surpassing the T_c value of the initial process. This shift gives rise to either normal or reversed hysteresis loops (Fig. 1).

This leads to a fundamental question: are normal and reverse hysteresis the only possible behaviors in SCO systems? Could a process exist in which the critical temperatures for heating and cooling are exchanged, creating an "inverted" hysteresis?

An analogy can be drawn to the field of molecular magnets, where the dependence of magnetization on an external magnetic field typically forms a counterclockwise hysteresis loop. However, there are known examples of "inverted" hysteresis, in which the magnetization *vs.* field curve evolves clockwise.[13–16] Nevertheless, such an "inverted" thermal hysteresis phenomenon has remained unprecedented within the field of spin crossover compounds.

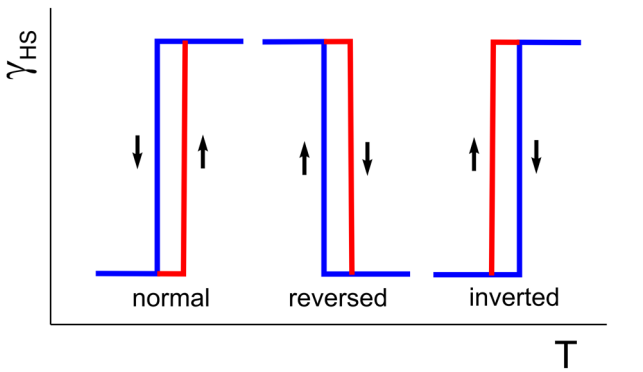

Fig. 1 Schematic presentation of hysteresis: "normal" (a), "reversed" (b), and "inverted" (c). Blue corresponds to cooling whereas red corresponds to heating.

In this communication, we demonstrate the feasibility of an SCO transition that follows an "inverted" thermal hysteresis pattern. This phenomenon was discovered using the stearate ester of 2-hydroxy-1,3-di(1*H*-1,2,3-triazol-1-yl)propane (**L1**) as the ligand system (Fig. S1). The synthesis of the crystalline compound $[Fe(\mathbf{L1})_4](BF_4)_2{\cdot}\mathbf{L1}{\cdot}2CH_3CN{\cdot}0.23H_2O$ (**1**), obtained from the reaction of **L1** with iron(II) tetrafluoroborate in acetonitrile (see SI), proceeds extremely slowly. The formation of single crystals requires approximately one year and necessitates multiple parallel syntheses.

In **1**, two of five **L1** molecules (denoted C300/C600 and C200) act as bridging ligands. They link Fe(II) ions separated along the [−110] direction at a distance of 9.697(3) Å (250 K), leading to the formation of a polymeric chain (Fig. 2). The alkyl side chain of one of the two bridging molecules (C300/C600) is disordered, with a site occupancy ratio of 0.58 : 0.42.

The next two molecules (C100 and C400) are coordinated monodentately and are ordered. The fifth ligand molecule (C900) remains uncoordinated. The coordination environment

Faculty of Chemistry, University of Wrocław, F. Joliot-Curie 14, 50-383, Wrocław, Poland. E-mail: robert.bronisz@uwr.edu.pl

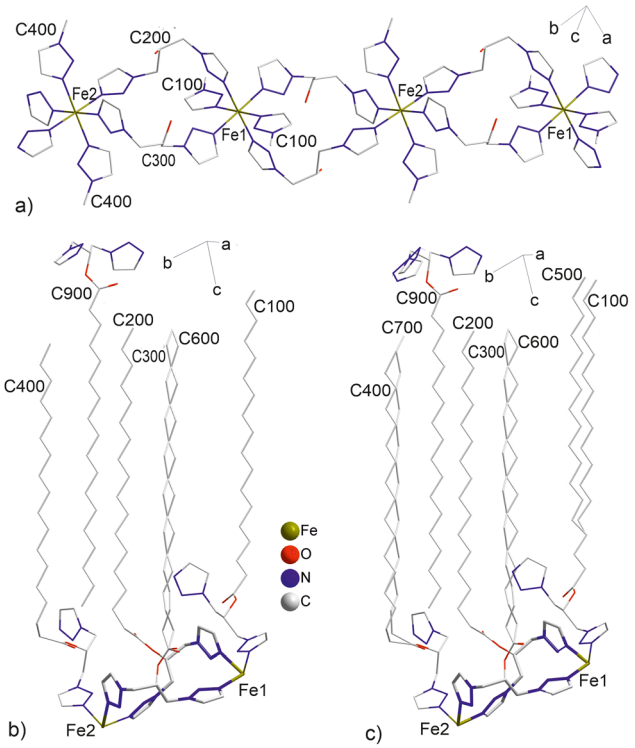

Fig. 2 Structure of the polymeric chain together with coordination modes (a), conformations of **L1** molecules in the HS form ((b) 250 K) and in the LS form ((c) 80 K) of **1**. The 1,3-di(1,2,3-triazol-1-yl)propylene fragments of bridging molecules are highlighted with thick lines (b) and (c). Counterions, acetonitrile, water molecules, and hydrogen atoms have been omitted for clarity.

of Fe(II) ions is composed of 1,2,3-triazole rings coordinating through N3 nitrogen atoms.

At 250 K, the Fe1–N distances range from 2.167(2) to 2.188(2), whereas Fe2–N distances are slightly longer, with values between 2.194(5) and 2.210(2). The N–Fe–N angles are similar for both sites, ranging from 89 to 91°. Thus, the coordination sphere of Fe(II) is suitable for the occurrence of SCO.

Neighboring polymeric chains, assembled within the *ab* plane, are separated at a distance of 12.1 Å, forming polar layers (Fig. 3). Disordered anions and acetonitrile molecules occupy the intralayer spaces (Fig. S2). The C17 side alkyl chains, oriented in the same direction, form a distinct lipophilic

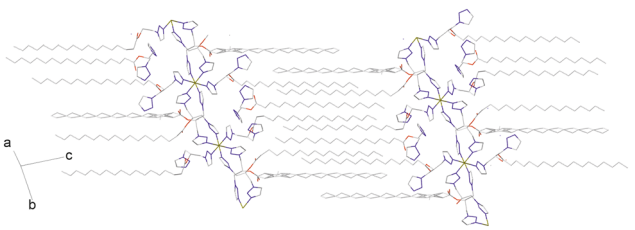

Fig. 3 Structure of **1** at 250 K, showing polymeric chains and bilayer arrangement. Counterions, acetonitrile and water molecules, and hydrogen atoms are omitted for clarity.

domain between the polar layers. Upon further temperature increase, the $\chi_M T$ value rises more rapidly than in the cooling mode. Consequently, the $\chi_M T$ values measured upon heating are consistently higher than those obtained at the same temperature during cooling. This divergence becomes progressively more pronounced with increasing temperature, reaching a maximum at 173 K.

Compound **1** remains in the HS state at room temperature. Upon cooling of fine crystalline sample 1 (1 K min^{-1}), the $\chi_M T$ value decreases slightly between 230 K and 190 K (Fig. 4a). Further cooling leads to a distortion of the SCO curve, and a narrow step appears between 171 K ($\chi_M T$ = 1.90 cm^3 kmol^{-1}) and 161 K ($\chi_M T$ = 1.76 cm^3 kmol^{-1}). Below this step, the slope of the $\chi_M T(T)$ dependence is restored, and SCO is completed at 60–70 K.

During heating, up to approximately 110–120 K, the $\chi_M T(T)$ dependence follows the same path as recorded during cooling.

At this temperature, $\chi_M T$ = 2.12 cm^3 kmol^{-1} during heating, compared to 1.91 cm^3 kmol^{-1} during cooling. Above 190 K, the heating curve overlaps the cooling curve. These results demonstrate that the cooling/heating cycle forms an "inverted" hysteresis loop, in contrast to the typically observed "normal" hysteresis (Fig. 1). At its widest point, corresponding to $\chi_M T$ = 1.90 cm^3 kmol^{-1}, the width of the "inverted" hysteresis is approximately 8 K ($T_{1/2}{}^{\downarrow}$ = 178 K; $T_{1/2}{}^{\uparrow}$ = 170 K).

Isothermal $\chi_M T$ measurements were performed for the second sample (crystalline) at 140, 150, 160, 170, 180, and 190 K (Fig. 4b and Fig. S3). At each temperature, data were recorded for 240

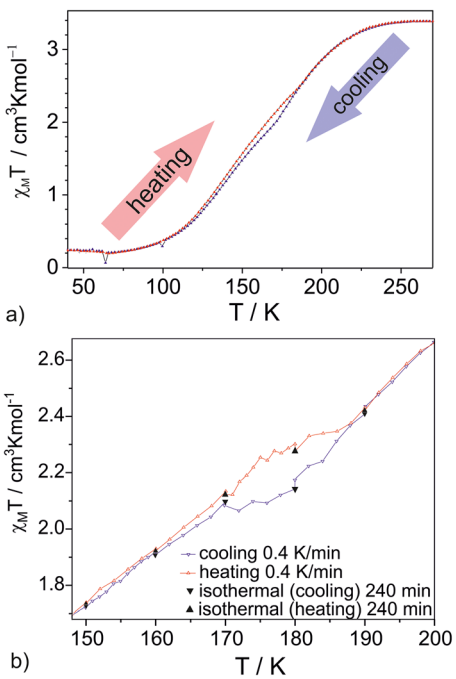

Fig. 4 $\chi_M T(T)$ dependence recorded for sample 1 in cooling (blue) and heating (red) mode at 1 K min^{-1} (a), and $\chi_M T(T)$ dependence recorded for sample 2 in isothermal mode (cooling—black up triangles, heating—black down triangles) at 150, 160, 170, 180, and 190 K (the temperature was changed between these points at a rate of 0.4 K min^{-1}, open symbols) (b).

minutes. The temperature between points was changed at a rate of 0.4 K min^{-1}. Under these conditions, the "inverted" hysteresis loop is still present, but it is shifted to slightly higher temperatures. Measurements performed for sample 3 (fine crystalline) at 1, 2, and 4 K min^{-1} confirmed the presence of an "inverted" hysteresis loop (Fig. S4).

Differential scanning calorimetry (DSC) was performed on the same crystalline sample used for the SC-XRD studies. The measurement revealed an anomalous thermal effect, with onset temperatures estimated at 177 K (cooling) and 182 K (heating) at a rate of 10 K min^{-1} (Fig. S5). Given the broad temperature range of SCO, this effect cannot be attributed to the SCO process itself. Moreover, the endothermic peak (heating) is shifted to a higher temperature relative to the exothermic peak (cooling), which is characteristic of a normal hysteresis. Therefore, the observed thermal anomaly most likely originates from additional, distinct structural processes and does not result only from spin crossover.

SC-XRD studies performed at various temperatures revealed abrupt changes in the a and c as well as in the α and β lattice parameters within the 160–175 K temperature range (Fig. S6). Notably, the temperature dependence of the unit cell volume exhibits anomalous behavior. Within the 110–190 K range, two distinct stages can be identified, each displaying an "inverted" hysteresis (Fig. S7).

Below 190 K, an abrupt reorientation of the C100, C300, and C400 alkyl chains begins (Fig. 5 and Fig. S8). However, for the C100 and C300 chains, these conformational changes reverse upon cooling to 175 K. When the temperature is further lowered to 160 K, the site occupancy factors (SOFs) of the dominant conformers for C100 and C400 decrease significantly to 55–57%. These conformational alterations correlate with the abrupt changes observed in the lattice parameters.

Upon cooling within the 130–160 K range, a very slight increase in the SOFs of the C100, C300, and C400 conformers is observed, followed by a gradual reduction. In contrast, for the uncoordinated C900 molecule, no conformational changes of its alkyl chain are observed below 190 K; however, disordering of one of its two triazole rings emerges. Thus, the structural reorganization proceeds in distinct stages, presenting a picture that is more complex than that inferred from the magnetic and DSC data alone.

During heating, the conformational changes do not follow the same path as during cooling, and the temperature dependences of the SOFs for the individual conformers differ. In the 130–160 K range, the occupancy of the C100, C300, and C400 conformers is slightly higher than that recorded during cooling. In the 175–190 K range, the occupancy of the C100 and C300 conformers is greater compared to the cooling mode. Notably, the changes occurring in the 130–190 K range correlate with a larger unit cell volume observed during heating. In contrast, the C400 chain exhibits a normal hysteresis loop. Anions remain disordered over the entire temperature range (Fig. S9).

Two major conclusions can be drawn from the SC-XRD studies: (i) the structural environment of the Fe(II) centers undergoes continuous and non-monotonic perturbation during the thermally induced SCO, and (ii) the anomalous temperature dependences of both the lattice parameters and the conformers' contributions indicate that the properties of the crystal lattice preferentially stabilize the HS state during heating.

During cooling, the contribution of the HS form, associated with the Fe1 center, starts to decrease below 200 K quite rapidly (Fig. 6). At 175 K, the ⟨Fe1–N⟩ distance reaches 2.045 Å, indicating that *ca.* 75% of the Fe1 ions have converted to the LS state. In contrast, for the Fe2 site, the ⟨Fe2–N⟩ distance at 175 K is 2.168 Å, implying that only about 15% of the Fe(II) ions at this site have switched their spin state. The trend of decreasing Fe1–N bond lengths continues with temperature, and at 80 K, the individual Fe1–N distances are 1.987(2), 2.000(2), and 2.009(2) Å.

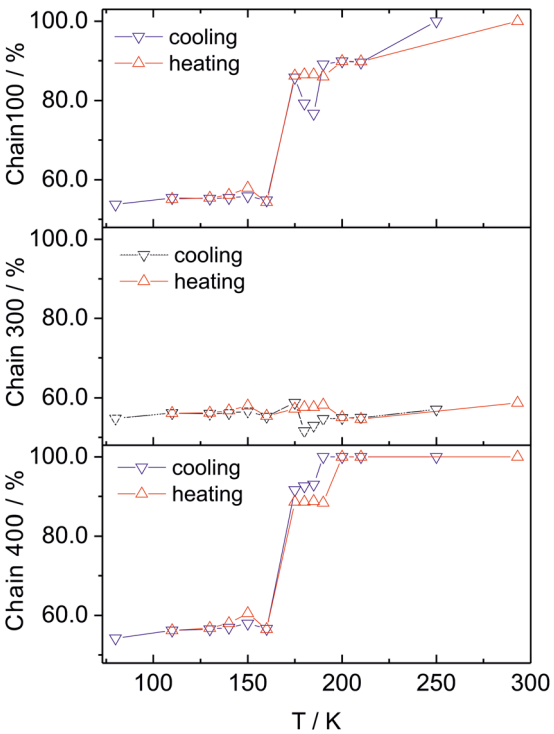

Fig. 5 Temperature dependence of the SOFs for the C100, C300, and C400 alkyl chains in **1**.

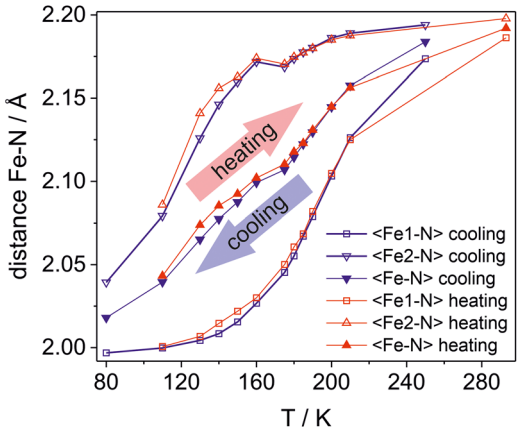

Fig. 6 Temperature dependence of the average Fe–N distances for the Fe1 site, the Fe2 site, and the global average ⟨Fe–N⟩ ((⟨Fe1–N⟩ + ⟨Fe2–N⟩)/2) recorded during cooling (blue) and heating (red).

The Fe2 center exhibits different behaviour. Cooling from 175 K to 160 K induces a reverse spin crossover, evidenced by a very slight increase in the ⟨Fe2–N⟩ distance to 2.172 Å. Upon further cooling, the ⟨Fe2–N⟩ distance begins to decrease again. At 80 K, the Fe2–N bond lengths (2.028(2), 2.032(2), and 2.045(2) Å) are slightly longer than those for Fe1, indicating a residual HS contribution of approximately 16% at the Fe2 site. Consequently, the overall average HS contribution from both Fe1 and Fe2 centers can be estimated to be about 8% at 80 K. This result is consistent with the magnetic data, which confirm the presence of a residual fraction of the HS form.

Heating from 80 K induces a rapid increase in the ⟨Fe2–N⟩ bond length, whereas the ⟨Fe1–N⟩ distance remains nearly constant up to 120–130 K. As the temperature continues to rise, the ⟨Fe1–N⟩ bond length undergoes significant elongation, with the transition becoming more abrupt above 160–175 K. In contrast, for the Fe2 centers, an anomaly is reproduced in the 160–175 K range, manifesting as a ''reverse'' SCO event. For the Fe2 site, increasing the temperature from 175 K to 250 K results only in a further, very slight increase in the ⟨Fe2–N⟩ distance.

A comparison of the Fe–N bond length evolution during cooling and heating for the Fe1 and Fe2 sites confirms their atypical behavior. The data reveal that both the ⟨Fe1–N⟩ and ⟨Fe2–N⟩ values are consistently greater during the heating cycle than at the corresponding temperatures during cooling. As this phenomenon occurs for both independent spin crossover centers, the globally averaged ⟨Fe–N⟩ bond length is consequently greater during heating (Fig. 6). This effect is most pronounced in the 130–180 K temperature range.

The results of SC-XRD and magnetic studies consistently indicate the occurrence of ''inverted'' hysteresis. The complex nature of the structural changes and the relative subtlety of the effect do not allow for a definitive identification of the responsible mechanism. Nevertheless, we believe the observed phenomenon can be broken down into elementary processes and described as a combination of a normal spin crossover and a reverse transition (see SI, Fig. S10).

Critically, the results of SC-XRD studies directly corroborate the observations from magnetic measurements. This agreement definitively excludes a change in the orbital angular momentum (orbital angular momentum crossover)[17–20] as the mechanism responsible for the observed ''inverted'' hysteresis.

In conclusion, the 1D coordination polymer $[Fe(\mathbf{L1})_4](BF_4)_2\cdot\mathbf{L1}\cdot 2CH_3CN\cdot 0.23H_2O$, featuring a bilayer lipophilic/polar architecture, exhibits a complete, thermally induced spin crossover HS ⇄ LS that is intricately coupled to complex conformational changes of the entire C17 alkyl chains. The resulting ''inverted'' hysteresis represents a fundamentally distinct behavior. It does not correspond to either the known ''normal'' or ''reverse'' SCO scenarios, in which the HS → LS transition curve is invariably shifted toward the stability region of the LS form (Fig. 1). Instead, this system inverts that relationship, establishing a novel, structurally confirmed paradigm in spin crossover phenomena.

A. T. ligand and complex synthesis, analysis and data interpretation, results presentation. M. K. FTIR data collection. DSC analysis. M. K., V. M., and M. S. planning SC-XRD studies. V. M. and M. S. crystal structure determination and data analysis. M. W. magnetic susceptibility data collection. R. B. supervision, financial support, manuscript preparation.

Conflicts of interest

There are no conflicts to declare.

Data availability

The data supporting this article have been included as part of the supplementary information (SI). Supplementary information is available. See DOI: https://doi.org/10.1039/d6cc00357e.

CCDC 2515367–2515369 contain the supplementary crystallographic data for this paper.[21a–c]

References

1 P. Gütlich, A. Hauser and H. Spiering, *Angew. Chem., Int. Ed. Engl.*, 1994, **33**, 2024.
2 A. Halcrow, *Spin-Crossover Materials: Properties and Applications*, Wiley-VCH, Weinheim, 2013.
3 M. Sorai and S. Seki, *J. Phys. Chem. Solids*, 1974, **35**, 555.
4 W. Nicolazzi and A. Bousseksou, *C. R. Chim.*, 2018, **21**, 1060.
5 R. Akiyoshi, R. Ohtani, L. F. Lindoy and S. Hayami, *Dalton Trans.*, 2021, **50**, 5065.
6 S. Hayami, M. R. Karim and Y. H. Lee, *Eur. J. Inorg. Chem.*, 2013, 683.
7 A. B. Gaspar, M. Seredyuk and P. Gütlich, *Coord. Chem. Rev.*, 2009, **253**, 2399.
8 G. Agustí, C. Bartual, V. Martínez, F. J. Muñoz-Lara, A. B. Gaspar, M. C. Muñoz and J. A. Real, *New. J. Chem.*, 2009, **33**, 1262.
9 M. Weselski, M. Książek, P. Mess, J. Kusz and R. Bronisz, *Chem. Commun.*, 2019, **55**, 7033.
10 M. Weselski, M. Książek, D. Rokosz, A. Dreczko, J. Kusz and R. Bronisz, *Chem. Commun.*, 2018, **54**, 3895.
11 M. Seredyuk, M. C. Munoz, M. Castro, T. Romero-Morcillo, A. B. Gaspar and J. A. Real, *Chem. – Eur. J.*, 2013, **19**, 6591.
12 F. J. Valverde-Muñoz, M. Seredyuk, M. Meneses-Sánchez, M. C. Muñoz, C. Bartual-Murguia and J. A. Real, *Chem. Sci.*, 2019, **10**, 3807.
13 D. Belo and M. Almeida, *Coord. Chem. Rev.*, 2010, **254**, 1479.
14 P. P. Shen, Y. T. Wang and B. A. Sun, *Front. Mater.*, 2021, **8**, 765427.
15 I. Soldatov, P. Andrei and R. Schaefer, *IEEE Magn. Lett.*, 2020, **11**, 2405805.
16 T. Maity, D. Kepaptsoglou, M. Schmidt, Q. Ramasse and S. Roy, *Phys. Rev. B*, 2017, **95**, 100401(R).
17 G. Juhász, R. Matsuda, S. Kanegawa, K. Inoue, O. Sato and K. Yoshizawa, *J. Am. Chem. Soc.*, 2008, **131**, 4560.
18 H. Zenno, R. Akiyoshi, M. Nakamura, G. G. Morgan and S. Hayami, *Chem. Lett.*, 2020, **49**, 1099.
19 F. Kobayashi, Y. Komatsumaru, R. Akiyoshi, M. Nakamura, Y. Zhang, L. F. Lindoy and S. Hayami, *Inorg. Chem.*, 2020, **59**, 16843.
20 S. Q. Su, S. Q. Wu, M. L. Baker, P. Bencok, N. Azuma, Y. Miyazaki, M. Nakano, S. Kang, Y. Shiota, K. Yoshizawa, S. Kanegawa and O. Sato, *J. Am. Chem. Soc.*, 2020, **142**, 11434.
21 (*a*) CCDC 2515367: Experimental Crystal Structure Determination, 2026, DOI: 10.5517/ccdc.csd.cc2qffwh; (*b*) CCDC 2515368: Experimental Crystal Structure Determination, 2026, DOI: 10.5517/ccdc.csd.cc2qffxj; (*c*) CCDC 2515369: Experimental Crystal Structure Determination, 2026, DOI: 10.5517/ccdc.csd.cc2qffyk.

